A Balanced Bandpass Filter with High-Selectivity and Common-Mode Suppression Based on Inverted Microstrip Gap Waveguide

Feng Wei, Xing-Chen Zhou, Zeng-Hui Shi, Hong-Yu Liu, Pei-Yuan Qin

***Abstract*—In this letter, a balanced bandpass filter (BPF) is reported by stacking two cavity resonators based on inverted microstrip gap waveguide (MGW). The proposed balanced feed structure achieves deep and wide common-mode (CM) suppression for the first time in a gap waveguide (GW) structure based on a mushroom-type electromagnetic bandgap (EBG) cell package. A highly selective balanced fourth-order bandpass response with three out-of-band transmission zeros (TZs) and CM suppression are achieved by employing a pin-loaded patch perturbation structure at the center of the upper and lower cavities and a pair of slots on the common ground. A prototype of the stacked GW balanced BPF exhibiting a high selectivity was fabricated and measured. The measured results are in good agreement with the simulated ones.**

***Index Terms*—Balanced bandpass filter (BPF), common-mode (CM) suppression, inverted microstrip gap waveguide (MGW), high selectivity.**

I. Introduction

Balanced filters, characterized by their inherent noise suppression and intrinsic filtering properties, play a crucial role in enhancing the performance of balanced systems [1]-[4]. Microstrip lines are one of the classic transmission lines used in balanced bandpass filters (BPFs) [5]-[7]. However, the microstrip line has a large surface wave loss and dielectric loss at high frequencies. Consequently, substrate integrated waveguides (SIWs) and gap waveguides (GWs) have received much attention at higher frequencies. SIW is also one of the common transmission lines in balanced BPFs [8]-[11]. But, there is also some unavoidable dielectric losses in SIW.

Prior to the present work, some BPFs based on GWs have been proposed and the most of them are single-ended designs [12-20]. Compared with [19], the proposed BPF in this letter also achieves high selectivity, and more importantly, the balanced feed structure is first introduced into the inverted microstrip gap waveguide (MGW) BPF. Moreover, inherent broadband common-mode (CM) suppression is achieved.

According to the best we know, only the literature [20] has taken CM interference into account. Despite the fact that [20] demonstrates effective CM suppression, the BPF response does not produce transmission zeros (TZs) and exhibits suboptimal passband selectivity. Consequently, a GW BPF that combines both CM suppression and high selectivity is required.

Feng Wei, Xing-Chen Zhou, Zeng-Hui Shi and Hong-Yu Liu are with National Key Laboratory of Radar Detection and Sensing, Xi'an Key Laboratory of Millimeter Wave and Terahertz Technologies, Xidian University, Xi'an 710071, China (e-mail: fwei@mail.xidian.edu.cn).

Pei-Yuan Qin is with the Global Big Data Technologies Centre, University of Technology Sydney, Ultimo, NSW 2007, Australia (e-mail: pyqin1983@hotmail.com).

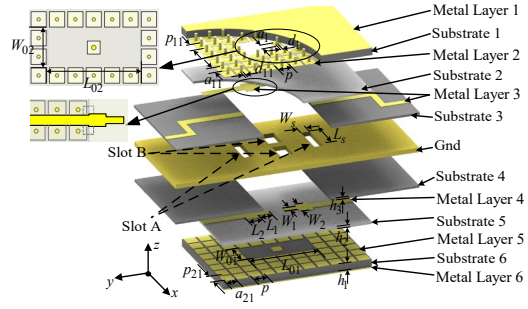

(a)

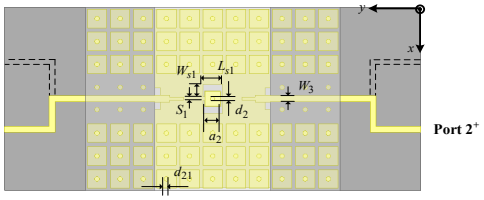

(b)

Fig. 1. 3-D layout and top-view schematic of the proposed balanced BPF with dimensions $a_{11} = a_{21} = 2.95$, $d_{11} = 0.6$, $d_{21} = 0.6$, $p = 3.05$, $p_{11} = 3.1$, $p_{21} = 3.07$, $a_1 = 1.95$, $a_2 = 2.15$, $d_1 = 0.5$, $d_2 = 0.8$, $W_s = 1$, $L_s = 4$, $L_{s1} = 3$, $W_{s1} = 3$, $S_1 = 0.25$, $W_1 = 0.4$, $W_2 = 1$, $W_3 = 0.8$, $L_1 = 1.8$, $L_2 = 2$, $L_{01} = L_{02} = 15.35$, $W_{01} = 6.26$, $W_{02} = 6.35$ (unit: mm). (a) 3-D layout. (b) Top-view schematic.

In this letter, a high selectivity balanced BPF is proposed. The electric field distribution and boundary conditions of a slot line are used with a pair of back-to-back microstrip lines to form a balanced feed structure that achieves good CM suppression. Meanwhile, a pin-loaded patch structure and a pair of slots are introduced into the cavity in order to improve the selectivity of the BPF. The balanced BPF is designed and fabricated.

II. Design of the Balanced BPF

Fig. 1 illustrates the 3-D layout and top-view schematic of the proposed balanced BPF. As shown in the Fig.1, the balanced BPF consists of two vertically stacked cavity resonators and a pair of balanced ports. The balanced ports consist of four back-to-back microstrip lines and a pair of slots called slot A orthogonal to them. An h = 1mm copper plate was used as the common ground for the two cavity resonators. The cavity resonator is obtained by removing the 2×5 electromagnetic bandgap (EBG) units from the central region and setting three rows of EBG units around to suppress the leakage of electromagnetic (EM) energy. The resonant mode can be determined through the method described in [19]. In this letter, the TE_{102} and TE_{103} modes are utilized. Furthermore, the pin-loaded patches at the center of the bottom layer are used to

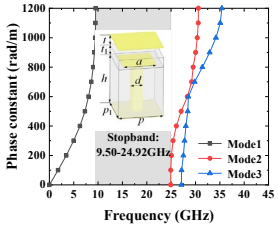

Fig. 2. Extracted dispersion diagram of the used mushroom-type EBG cell of the IMGW in Fig. 1 with dimensions a = 2.6, d = 0.5, p_1 = 3.1, p = 3.05, h = 1.575, and $t = t_1$ = 0.254 (unit: mm).

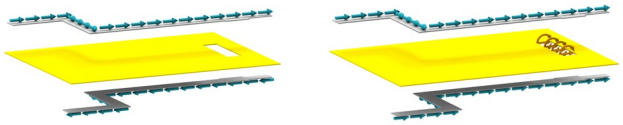

(a) (b)

Fig. 3. Current distribution of microstrip lines of the BFS and electric field distribution of slot A of the balanced structure under (a) DM and (b) CM excitation.

generate transmission passbands and TZs [19]. A pair of slots for enhancing the magnetic coupling strength is added to the common ground, i.e., slot B. All dielectric substrates have a dielectric constant ε_r = 2.2 and loss tangent tan (δ_D) = 0.0009.

Fig. 2 displays the dispersion diagram associated with the EBG unit cell. The stopband range of the EBG is identified to extend from 9.50 GHz to 24.92 GHz. And the BPF response is meticulously designed to coincide with the aforementioned stopband range. The EBG unit used in this work is a rectangular one, and the size of the upper and lower cavities is adjusted mainly by adjusting the p_1 parameter in the x-direction.

A. Balanced feed structure

The proposed balanced feed structure is demonstrated in Fig. 1. Slot A is etched into the common ground orthogonally relative to the feeding lines, as illustrated in Fig. 1.

During differential-mode (DM) excitation, Port 1^+ and Port 1^- carry signals with equal amplitude but opposite phase, as shown in Fig. 3(a). Due to the symmetrical arrangement of the balanced feed structure around the y-axis, the behavior of the common ground at this junction is therefore similar to that of a perfect electrical conductor (PEC), with the PEC boundary conditions delineated in (1):

$$\frac{\partial E_n}{\partial n} = 0,\ E_t = E_l = 0,\ Z_t = Z_l = 0. \tag{1}$$

Thus, under DM excitation, the electric field distribution of the balanced feed structure does not align with the boundary conditions of slot A; consequently, the balanced feed structure and slot A are unassociated, as depicted in Fig. 3(a).

Under CM excitation, the signals at Port 1^+ and Port 1^- exhibit equal amplitude and are in phase, as shown in Fig. 3(b). This figure reveals that, at this point, the common ground plane effectively serves as a perfect magnetic conductor (PMC) plane. The associated boundary conditions for the PMC are specified in (2):

$$\frac{\partial E_l}{\partial n} = \frac{\partial E_t}{\partial n} = 0,\ E_n = 0,\ Z_t = Z_l = \infty. \tag{2}$$

Therefore, under CM excitation, the balanced feed structure electric field distribution matches the boundary conditions of

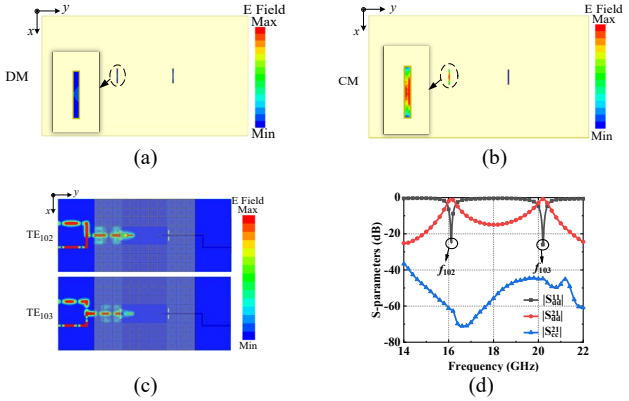

Fig. 4. RF characteristics of the proposed BPF (the cavities of upper and lower resonator are same) without the pin-loaded patch perturbation and slot B. (a) Simulated E-field distributions of the slot A under DM and (b) CM excitation. (c) Simulated E-field distributions for f_{102} at 16.13 GHz and f_{103} at 20.16 GHz under CM excitation. (d) Simulated S-parameters of the proposed BPF (the cavities of upper and lower resonator are same) without the pin-loaded patch perturbation and slot B.

slot A, resulting in the excitation of slot A, as shown in Fig. 3(b).

In agreement with the theoretical analysis, Fig. 4(a) and (b) show the electric field distribution of slot A simulated under DM and CM excitation, respectively. When slot A is excited, a loop is constituted at the microstrip line at Port 1^+ with slot A and the microstrip line at Port 1^-. The energy is imparted from Port 1^+/1^- to form a resonance at slot A, as shown in Fig. 4(b). The electric field resonating in situ at slot A is unable to radiate energy efficiently into the cavity, and therefore is unable to excite the cavity, and CM suppression is achieved.

Fig. 4(c) indicates the electric field distribution at f_{102} and f_{103} under CM excitation. As shown in Fig. 4(c), the electric field is distributed at the microstrip lines of 1^+ and 1^- ports and at slot A. There is no electric field distribution in the cavity. The proposed balanced feed structure therefore exhibits robust CM suppression, the frequency response of which is presented in Fig. 4(d).

B. Design of the proposed BPF with high selectivity

Fig. 4(d) shows the simulated S-parameters of the balanced BPF comprising two same cavity resonators arranged in a vertically stacked structure, which shows an excellent CM suppression effect. To achieve the single-passband filtering response, a pin-loaded patch is introduced as a perturbation in the center of the bottom and top periodically aligned mushroom-type EBG structures, respectively, and a pair of slots (i.e., slot B) is etched on a common ground.

The cavity perturbation theory indicates that the pin-loaded patch affects the distribution of the electric field in the TE_{103} mode, while having no influence on the TE_{102} mode. It can be deduced that the f_{103} can be adjusted by adjusting the size of the pin-loaded patch, while not affecting the f_{102}. From the doublet coupling, the expectation is that a TZ will be generated by a filter based on cavity resonator (with the pin-loaded patch) [21].

The variation curves of the frequencies of transmission poles (TPs) (TP_1 and TP_2) and a TZ of the different values of a_1 and d_1 are given in Fig. 5. As can be seen, both the TZ and TP_2 (i.e., the resonant frequency f_{103} corresponding to the TE_{103} mode) shift towards lower frequency as the parameter a_1 increases or d_1 decreases. At the same time, the TP_1 (i.e., the resonant

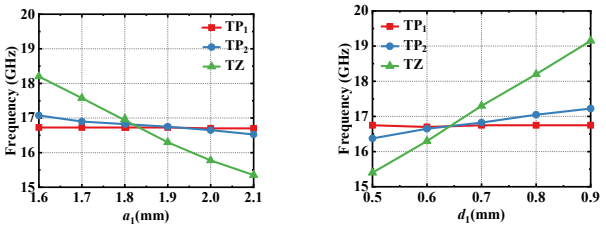

(a) (b)

Fig. 5. (a) Frequencies of TZ and TPs (TP_1 and TP_2) of the varied a_1 with d_1 = 0.8 mm. (b) Frequencies of TZ and TPs (TP_1 and TP_2) of the varied d_1 with a_1 = 2 mm.

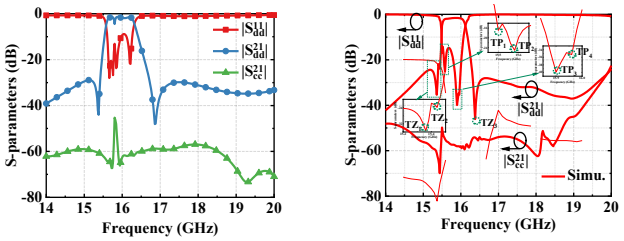

(a) (b)

Fig. 6. (a) Simulated S-parameters of the proposed BPF (the cavities of upper and lower resonators are different) without slot B. (b) Simulated S-parameters of the final optimized BPF (the cavities of upper and lower resonators are different) with slot B. (TP_1 corresponding to the f_{103} of the upper resonator, TP_2 corresponding to the f_{102} of the upper resonator, TP_3 corresponding to the f_{102} of the lower resonator, TP_4 corresponding to the f_{103} of the lower resonator.)

frequency f_{102} corresponding to the TE_{102} mode) remains essentially constant throughout the investigated range. Furthermore, regardless of whether f_{102} is greater than or less than f_{103}, the TZ consistently emerges on the side proximal to TP_2.

As illustrated in Fig. 1, the proposed final BPF prototype is constructed by cascading the upper and lower cavity resonators on a vertical stacking configuration. In order to obtain a fourth-order BPF response and to ensure balanced feed structure integrity (i.e., symmetry of the balanced feed lines about the common ground), the periods in the x-axis direction of the upper and lower EBG units (i.e., p_{11}, p_{21}) are inconsistent. As a result, the cavities of the upper and lower have different dimensions, thereby separating the f_{102} of the two resonators. Furthermore, the pin-loaded patch parameters of the upper and lower cavity resonators are adjusted separately so that the TZ generated by the large (i.e., upper) resonator is situated on the below side of the passband, and the TZ generated by the small (i.e., lower) resonator is located on the above side of the passband. Unfortunately, as seen from the simulated S-parameters depicted in Fig. 6(a), an additional in-band TZ which destroys the filtering performance is generated due to the difference sizes of the two cavities. Please note that the slot B structure has not been introduced at this time. The relationship between the position f_z of this TZ and the filter center frequency f_0 is as follows:

$$\frac{f_0}{f_z} = \sqrt{\frac{M_c}{E_c}} \tag{3}$$

Wherein M_c and E_c represent the magnitudes of magnetic and electric couplings, respectively [22]. In order to obtain a fourth-order balanced BPF with perfect filtering, a pair of slots called slot B is etched into the central of the common ground. The introduction of slot B is used to enhance the magnetic coupling strength between the two resonant cavities without having

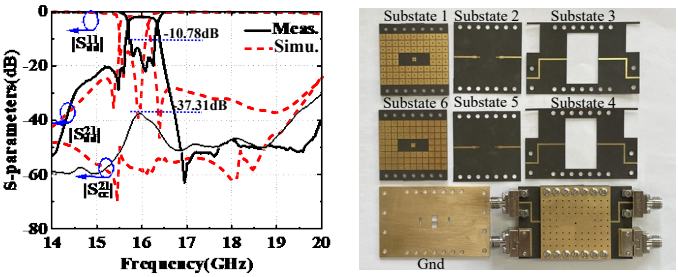

(a) (b)

Fig. 7. (a) Simulated and measured S-parameters of the final proposed balanced BPF. (b) Photographs of the final proposed balanced BPF.

TABLE I
PERFORMANCE COMPARISON WITH SIMILAR WORKS

Ref.	FBW/ f_0 (GHz)/ IL (dB)	TZs	CMS	CMS band	Size ($\lambda_g \times \lambda_g$)	DT
[8]	6.5*%/10.2 /2	0	Yes	4GHz @36dB	1.65×0 .96	SIW
[13]	5.5%/14.8/ 1.35	/	No	/	3.29×2 .16	GW
[15]	2.3%, 2.2% /13.68, 19.12/3.5, 3.1	0	No	/	1.85×1 .85	GW
[20]	1%/14/0.8*	0	Yes	5GHz @50dB	2.18×1 .43	GW
This Work	**3.5%/15.8/ 1.93**	**3**	**Yes**	**7.15GHz @37.13dB**	**3.75×1 .81**	**GW**

CMS: common-mode suppression; *: estimated from graphs; DT: design technology.

essentially any effect on the electrical coupling strength. With Eq. (3), as M_c increases, f_z decreases.

Therefore, the in-band TZ shown in Fig. 6 is tuned to the lower edge of the passband by adjusting the dimensions of the slot B and a corresponding adjustment in its position. Fig. 6(b) demonstrates the frequency response of the final optimized BPF. Among them, the four in-band TPs (TP_1, TP_2, TP_3, TP_4) correspond to the TE_{103} mode and TE_{102} mode of the upper cavity and TE_{102} mode and TE_{103} mode of the lower cavity, respectively. The three out-of-band TZs of the ceramic bowl are obtained while the CM suppression is better than 50 dB.

To validate the practicability of the proposed filter's structure illustrated in Fig. 1, the prototype of the balanced BPF is fabricated and measured. Fig. 7(a) shows the measured results as well as a photograph of the assembled balanced BPF. The key performance metrics of the balanced BPF measured in Fig. 7(a) are as follows: center frequency of 15.80 GHz, 3-dB fractional bandwidth (FBW) of 3.5%, in-band minimum insertion-loss level of 1.93 dB and the CM suppression better than 37.31 dB from 12.32 GHz to 19.47 GHz. The proposed BPF is compared with other balanced SIW or GW filters in Table I. It is clear that the BPF is competitive in terms of DM selectivity and CM suppression.

III. CONCLUSION

A balanced BPF with high-selectivity and CM suppression based on inverted MGW is proposed. The proposed balanced feed structure achieves good CM suppression for the first time based on inverted MGW, while a passband with three TZs is achieved by using a stack of two cavity resonators as well as a coupling gap.

REFERENCES

[1] P. Chu et al., "Balanced substrate integrated waveguide filter," in *IEEE Trans. Microw. Theory Techn.*, vol. 62, no. 4, pp. 824-831, April 2014.

[2] A. A. Coskun and A. Atalar, "Noise figure of a balanced amplifier," in *IEEE Trans. Circuits Syst. II, Exp. Briefs*, vol. 65, no. 9, pp. 1129-1133, Sept. 2018.

[3] J. -X. Chen, Y. Xue, X. Shi, Y. -X. Huang, W. Qin and Y. -J. Yang, "Design of double-ridge waveguide balanced filter and filtering power divider," in *IEEE Trans. Microw. Theory Techn.*, vol. 72, no. 10, pp. 5929-5937, Oct. 2024.

[4] B. Li and K. W. Leung, "On the differentially fed rectangular dielectric resonator antenna," in IEEE *Trans. Antennas Propag.*, vol. 56, no. 2, pp. 353-359, Feb. 2008.

[5] X. -B. Zhao, F. Wei, L. Yang and R. Gómez-García, "Two-layer-magic-T-based bandpass, quasi-bandstop, and dual-passband balanced filters with differential-/common-mode reflectionless behavior," in *IEEE Trans. Microw. Theory Techn.*, vol. 72, no. 4, pp. 2267-2282, April 2024.

[6] F. Wei, Y. -C. Xue, X. -B. Zhao, W. -S. Liu, L. Xu and P. F. Zhang, "Balanced BPF with dual-port quasi-reflectionless characteristic and selectivity enhancement," in *IEEE Trans. Circuits Syst. II, Exp. Briefs*, vol. 70, no. 3, pp. 994-998, March 2023.

[7] X. Guo, L. Zhu and W. Wu, "Strip-loaded slotline resonators for differential wideband bandpass filters with intrinsic common-mode rejection", in *IEEE Trans. Microw. Theory Techn.*, vol. 64, n.2, pp. 450-458, Feb. 2016.

[8] L. Sun, H. -W. Deng, Y. -F. Xue, J. -M. Zhu and S. -B. Xing, "Compact-balanced BPF and filtering crossover with intrinsic common-mode suppression using single-layered SIW cavity," in *IEEE Microw. Wireless Compon. Lett.,* vol. 30, no. 2, pp. 144-147, Feb. 2020.

[9] Y. -K. Han, H. -W. Deng, J. -M. Zhu, S. -b. Xing and W. Han, "Compact dual-band dual-mode SIW balanced BPF with intrinsic common-mode suppression," in *IEEE Microw. Wireless Compon. Lett.*, vol. 31, no. 2, pp. 101-104, Feb. 2021.

[10] H. -W. Deng, Y. -K. Han, L. Sun, J. -M. Zhu and S. -B. Xing, "Multilayer dual-mode balanced SIW filter utilizing PEC–PMC characteristic for common-mode suppression," in *IEEE Microw. Wireless Compon. Lett.*, vol. 30, no. 9, pp. 865-868, Sept. 2020.

[11] H. Chu and J. -X. Chen, "Dual-band substrate integrated waveguide balun bandpass filter with high selectivity," in *IEEE Microw. Wireless Compon. Lett.*, vol. 24, no. 6, pp. 379-381, June 2014.

[12] M. Sharifi Sorkherizi and A. A. Kishk, "Self-packaged, low-loss, planar bandpass filters for millimeter-wave application based on printed gap waveguide technology," in *IEEE Trans. Compon., Packag., Manuf. Technol.*, vol. 7, no. 9, pp. 1419-1431, Sept. 2017.

[13] S. Birgermajer, N. Janković, V. Radonić, V. Crnojević-Bengin and M. Bozzi, "Microstrip-ridge gap waveguide filter based on cavity resonators with mushroom inclusions," in *IEEE Trans. Microw. Theory Techn.*, vol. 66, no. 1, pp. 136-146, Jan. 2018.

[14] M. Sharifi Sorkherizi and A. A. Kishk, "Fully printed gap waveguide with facilitated design properties," in *IEEE Microw. Wireless Compon. Lett.*, vol. 26, no. 9, pp. 657-659, Sept. 2016.

[15] J. -Y. Deng, M. -J. Li, D. Sun, L. -X. Guo and X. -H. Ma, "Compact dual-band inverted-microstrip ridge gap waveguide bandpass filter," in *IEEE Trans. Microw. Theory Techn.*, vol. 68, no. 7, pp. 2625-2632, July 2020.

[16] M. Rezaee and A. U. Zaman, "Groove gap waveguide filter based on horizontally polarized resonators for v-band applications," in *IEEE Trans. Microw. Theory Techn.*, vol. 68, no. 7, pp. 2601-2609, July 2020.

[17] T. Xiu et al., "Design of a compact and low-loss e-band filter based on multilayer groove gap waveguide," in *IEEE Microw. Wireless Compon. Lett.*, vol. 31, no. 11, pp. 1211-1214, Nov. 2021.

[18] J. -Y. Deng et al., "Ultracompact bandpass filter based on slow wave substrate integrated groove gap waveguide," in *IEEE Trans. Microw. Theory Techn.*, vol. 70, no. 2, pp. 1211-1220, Feb. 2022.

[19] Z. -H. Shi, F. Wei, L. Yang and R. Gómez-García, "High-selectivity inverted microstrip gap waveguide bandpass filter using hybrid cavity and stub-loaded ring resonant modes," in *IEEE Trans. Circuits and Syst. II, Exp. Briefs*, vol. 71, no. 1, pp. 146-150, Jan. 2024.

[20] A. K. Horestani and M. Shahabadi, "Balanced filter with wideband common-mode suppression in groove gap waveguide technology," in *IEEE Microw. Wireless Compon. Lett.*, vol. 28, no. 2, pp. 132-134, Feb. 2018.

[21] U. Rosenberg and S. Amari, "Novel coupling schemes for microwave resonator filters," in *IEEE Trans. Microw. Theory Techn.*, vol. 50, no. 12, pp. 2896-2902, Dec. 2002.

[22] Q. -X. Chu and H. Wang, "A compact open-loop filter with mixed electric and magnetic coupling," in *IEEE Trans. Microw. Theory Techn.*, vol. 56, no. 2, pp. 431-439, Feb. 2008.